Development of a Tailored Thyroid Gland Phantom for Fine-Needle Aspiration Cytology by Three-Dimensional Printing

Masayuki Baba, MD,[*,†] Keitaro Matsumoto, MD, PhD,*[*,†] Naoya Yamasaki, MD, PhD,*[*,†] Hisakazu Shindo, MD, PhD,*[*,†] Hiroshi Yano, MD, PhD,*[*] Megumi Matsumoto, MD, PhD,*[*] Ryota Otsubo, MD, PhD,*[*] Murray John Lawn, PhD,[†,‡] Naoto Matsuo,[†] Ikuo Yamamoto, (D. Eng),[†,‡] Shigekazu Hidaka, MD, PhD,*[*] and Takeshi Nagayasu, MD, PhD*[*,†]

[*]Department of Surgical Oncology, Nagasaki University Graduate School of Biomedical Sciences, Nagasaki, Japan; [†]Medical-Engineering, Hybrid Professional Development Center, Nagasaki University Graduate School of Biomedical Sciences, Nagasaki, Japan; and [‡]Department of Mechanical Science, Nagasaki University Graduate School, Nagasaki, Japan

BACKGROUND: Fine-needle aspiration cytology (FNAC) is a challenging and risky procedure for inexperienced clinicians to perform because of the proximity of the thyroid to the jugular veins, carotid arteries, and trachea. A phantom model for transfixion practice would help train clinicians in FNAC.

OBJECTIVE: To fabricate a tailored phantom with consideration for authenticity of size, touch, feel, and ultrasonographic (US) characteristics.

METHODS: A three-dimensional (3D) digital model of the human neck was reconstructed from computed tomography data of a subject. This model was used to create 3D-printed templates for various organs that require US visualization. The templates were injected with polymers that provided similar degrees of ultrasound permeability as the corresponding organs. For fabrication of each organ, the respective molds of organs, blood vessels, thyroid gland, and tumor were injected with the material. The fabricated components were then removed from the templates and colored. Individual components were then positioned in the neck mold, and agar gel was poured in. The complete phantom was then removed from the mold. Thereafter, 45 medical doctors and students performed ultrasound-guided FNAC using the phantom, following which they were queried regarding the value of the phantom.

RESULTS: The structure, US characteristics, and elasticity of the phantom were similar to those of the human subject. In the survey, all 45 participants replied that they found the phantom useful for FNAC training, and 30 medical students professed increased interest in thyroid diseases after using the phantom.

CONCLUSIONS: We successfully fabricated a tailored thyroid gland phantom for transfixion practice. As most of the phantom parts are injected in molds fabricated using a 3D printer, they can be easily reproduced once the molds are fabricated. This phantom is expected to serve as an effective and fully tailored training model for practicing thyroid gland transfixion. (J Surg Ed 74:1039-1046. ©2017 Published by Elsevier Inc. on behalf of the Association of Program Directors in Surgery)

KEY WORDS: fine-needle aspiration cytology, 3D printing, phantom, ultrasonographic characteristics

COMPETENCY: Medical Knowledge

INTRODUCTION

Ultrasound-guided puncture is currently used for preservation of vessels, drainage, and biopsy; it may be employed for any step of the medical procedure, from diagnosis through treatment. Gaining safe, convenient, and precise access to complicated organ structures requires a high level of technical skill and expertise. Acquisition of such skills is essential for inexperienced doctors, irrespective of the

Correspondence: Inquiries to Takeshi Nagayasu, Department of Surgical Oncology, Nagasaki University Graduate School of Biomedical Sciences, 1-7-1 Sakamoto, Nagasaki 852-8501, Japan; fax: (95) 819-7306; e-mail: nagayasu@nagasaki-u.ac.jp

pathology and specialization. The most convenient way to acquire skills in ultrasound-guided puncture in any area is by practicing with phantoms, which has led to the development of a wide range of phantoms.[1–3]

Fine-needle aspiration cytology (FNAC) is a necessary procedure for the clinical diagnosis of thyroid gland cancer. Current clinical guidelines recommend FNA for nodules of diameter 1.0 to 1.5 cm as well as for smaller nodules with suspicious ultrasonographic (US) features.[4–6] Training for FNAC for thyroid diseases is essential given that the procedure is technically challenging, particularly for inexperienced residents, because of the proximity of the thyroid to the jugular veins, carotid arteries, and trachea. Recent studies have correlated the increase in diagnostic rate of thyroid gland diseases with increase in training,[7] which further highlights the importance of practicing FNAC with a phantom. Although thyroid neck training phantoms are commercially available, their prohibitive cost is a limitation for repeated training. Therefore, a low-cost, fully tailored phantom is ideal and required for transfixion practice.

Three-dimensional (3D) printing, which is a type of "additive manufacturing", is now widely used in both academic and commercial institutions. Although 3D printers have been used to create fully tailored phantoms, the types of medically suitable materials that can be printed from a 3D printer are limited. Therefore, we believed that it was necessary to devise a unique approach to create a low-cost, fully tailored, elaborate thyroid gland phantom for transfixion training. The aim of this study was to develop a low-cost thyroid gland phantom using a hybrid of old (traditional mold-based fabrication) and new (direct 3D printing) manufacturing techniques.

MATERIALS AND METHODS

This study was approved by the Ethics Committee of Nagasaki University Hospital (approval no., 16042512). All patients provided written consent for participation.

Materials

The major components that need to be represented in a thyroid gland phantom are the cervical vertebrae, trachea, common carotid arteries, internal jugular veins, thyroid gland, tumor, and surrounding soft tissue. Molds for these components were created using a 3D printer and injected with ultrasound-permeable materials. The 3D-printed molds were composed of a photopolymerizable acrylic resin, and the injected components mainly comprised agar and sodium alginate (Table).

Because blood vessels and the tumor require the fabrication of low, narrow, durable, small structures, a 3% solution of high-strength agar (Ina Agar Karikorikan, Japan; 3 g agar in 100 mL water), which has approximately 5 times the strength/concentration of regular agar, was used for fabricating the phantom.

At the same time, ultrasound luminescence of the thyroid gland is relatively high, and the phantom gland needs to be mechanically strong enough to withstand transfixion. Therefore, sodium alginate, which has the same base material as agar—i.e., algae—was used in combination with agar. The composition of 200 mL gel was as follows: 5 g sodium alginate, 20 mL ethanol, 80 mL saline, 0.1 g tetrasodium pyrophosphate, 0.7 g dicalcium phosphate,

TABLE. Materials and Cost

Organ	Material	Cost
Vertebrae	Acrylic light polymerized resin (Velo clear R; 3D printed)	$70
Trachea		$10
Outer frame mold		$1500
Vessel mold		$30
Tumor mold		$10
Thyroid gland mold		$40
Vessel	Agar (Karikorikan R Ina) + saline	$0.1
Tumor		
Thyroid gland	Sodium alginate (KIMICA I-1GR) + ethanol + saline Tetrasodium pyrophosphate Dicalcium phosphate Glucono-δ-lactone + water Agar (Karikorikan R Ina) + water	$1
Surrounding soft tissue	Agar (Yamato R Ina) + ethanol Sodium alginate (WAKO500-600) + ethanol + water	$3

While the vertebrae and the trachea were directly printed using a 3D printer, the remaining parts were poured/injected into 3D-printed molds. Blood vessels and tumor were fabricated with agar, and the thyroid gland was fabricated using a variety of materials. The surrounding soft tissue was fabricated with agar with sodium alginate for regulation of ultrasound luminescence.

3D, three dimensional.

2.0 g glucono-δ-lactone, 50 mL water, and 1.5 g agar in 50 mL water.

Yamato agar (Ina Co. Ltd., Japan) has greater elasticity in comparison with other regular agar materials and was, therefore, used for fabrication of soft tissue. The composition of 1200 mL Yamato agar gel was as follows: 2 g sodium alginate in 50 mL ethanol; 30 g agar (3%) in 150 mL ethanol and 1000 mL water.

Procedure for Fabrication

The procedure for fabrication of the thyroid gland phantom is shown in Figure 1. A 3D digital model of the human neck was reconstructed from computed tomography (CT) data and output as a stereolithography file. Molds for cerebral vertebrae and trachea, which are ultrasound-reflective components, were directly printed using a 3D printer (Object 260, Stratasys no. 33201, Eden Prairie, MN) as described previously. Molds for the remaining organs, which are ultrasound-transparent to a certain degree and, therefore, viewable by US, were first created using a 3D printer. Then, polymers that provide a similar degree of ultrasound permeability as the corresponding organs were poured into the molds of blood vessels, thyroid gland, and tumor. The fabricated components were removed from the molds and colored as required. Paint on regions adjacent to blood vessels has the effect of increasing the luminescence around blood vessels, a feature similar to that observed in the elderly patients. Finally, the individual components were arranged and fixed in their correct positions within the neck mold (outer frame), which was composed of polymers with similar properties as soft tissues such as skin and subcutaneous fat.

Specific details regarding the procedure and time required for fabrication of the gel compound that enables sonographically authentic imaging of internal organs are as follows. Sodium alginate was stirred into alcohol to form a solution, which was then added to water and stirred. To form a gel, calcium phosphate and sodium pyrophosphate were added to this solution and mixed for approximately 1 minute. Glucono-δ-lactone was then added to adjust the gelling speed. Polymers thus prepared were poured into their respective molds and allowed to harden at room temperature for approximately 1 hour, following which the fabricated components were removed from their molds. Finally, the gel representing the soft tissue in which the organs are embedded was prepared as follows: a small quantity of sodium alginate was added to a solution of water and alcohol and mixed well. To this solution, agar was added and mixed over heat until it completely dissolved. The polymer thus prepared was poured into the template and refrigerated at −4°C for approximately 1 hour. Once hardened, the fabricated

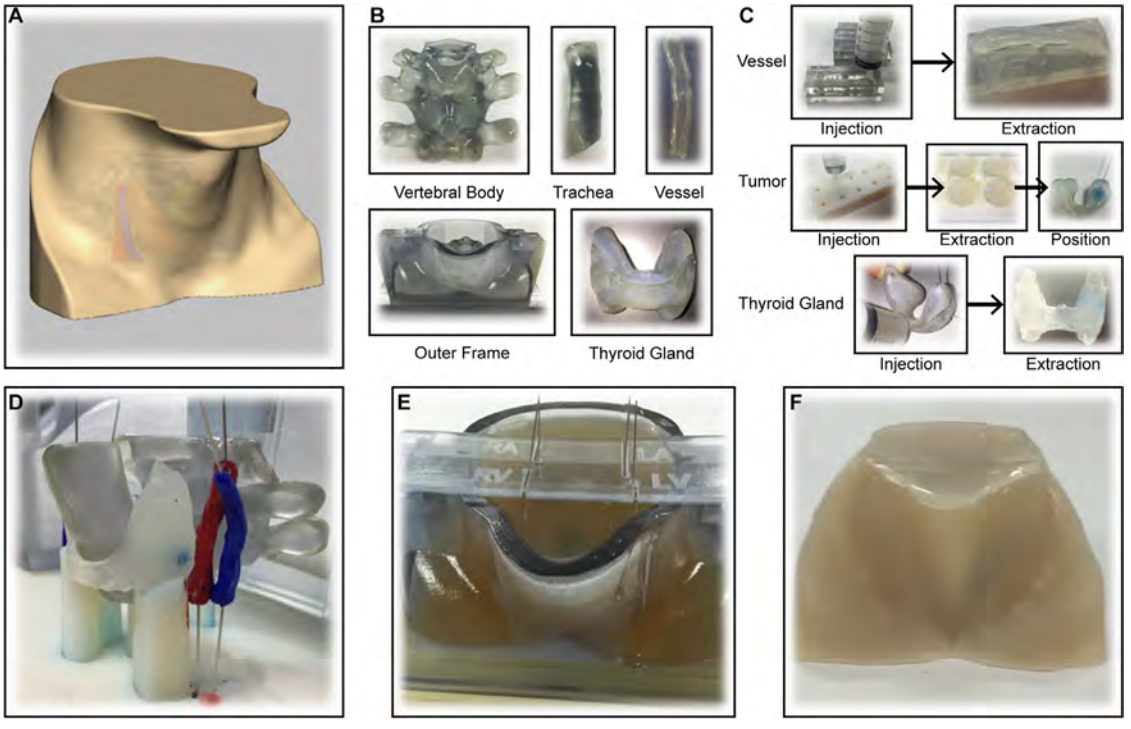

FIGURE 1. Order of construction. The protocol for fabrication of the neck mold is shown in (A)-(F), in order. Digitally reconstructed three-dimensional (3D) image (stereolithographic file) from computed tomography (CT) data (A); components/molds created by 3D printing (B); injection of materials into the molds (C); positioning of fabricated organs in the neck mold (D); pouring of materials into the neck mold with fabricated organs (E); and completed neck model (F).

component was removed from the mold, and the phantom thyroid gland was assembled and completed, ready for use. The size of the assembled phantom was approximately 20 × 10 × 10 cm, and it weighed approximately 1 kg. The phantom should be wrapped in cling film and refrigerated at −4°C to prevent degradation, mainly by drying. Although no preservatives were used in the fabrication process, the phantom exhibited no signs of visual or sonographic degradation for over 6 months.

Evaluation of Clinical Value of the Phantom

We asked 45 medical personnel—including 10 thyroid disease specialists, 8 senior and 12 junior residents, and 15 medical students—to perform FNAC using our thyroid phantom. After their use of our phantom, the participants were posed 2 questions—one regarding the usefulness of the phantom and the other querying whether there was a change in their interest in thyroid disease diagnosis and treatments after using this phantom.

Measurement

The phantom was evaluated using the LOGIQ e Premium (GE Healthcare, Chalfont Saint Giles, UK) US diagnostic unit. Luminescence was evaluated using the Image J 1.50 software.[8]

RESULTS

The assembled and completed neck phantom fabricated in this study is shown in Figure 1F. Its shape was similar to that of the model reconstructed from CT data (Fig. 1A).

Figure 2 presents US images of the human neck (Fig. 2A and C) and the thyroid gland phantom (Fig. 2B and D). The placement of organs was initially confirmed using these graphic data, because of which, each organ was located in its accurate position in the neck phantom. Muscle tissue was omitted from the phantom because the placement and fixation of muscles in an authentic manner for transfixion practice was very difficult. Although there were minor variations due to lack of consideration of muscle tissue, the phantom corresponded well with the human neck model in terms of shape, location, and US luminescence of organs, all of which are important factors in FNAC. In addition, the naturally narrow isthmus present between the right and left sides of the thyroid gland was designed to be thicker to ensure greater strength.

Luminescence in US images was evaluated using the Image J 1.50 software (Fig. 2E-H). In the histograms, the *x*-axis presents the spectrum of luminescence, and the *y*-axis presents the number of pixels for each value of luminescence. The total and mean pixel counts of the human thyroid gland were 957 and 124, respectively, whereas those of the phantom thyroid gland were 962 and 122, respectively (Fig. 2E and F). There were no differences in luminescence between the human and phantom thyroid glands. The total and mean pixel counts of blood vessels in the human neck were 870 and 15, respectively, whereas those of blood vessels in the phantom were 990 and 46, respectively (Fig. 2G and H). This difference in luminescence of blood vessels between the human neck and the phantom reflects the difference in luminescence between blood and agar. Furthermore, the phantom components were painted with different colors to differentiate the thyroid glands and blood vessels; this difference in color between the human neck and the phantom might have also contributed to the difference in luminescence. However, as blood vessels are readily identified by US, the difference in luminescence does not pose a significant issue for transfixion training.

To ensure that the phantom can be reused, it is important to determine whether the trajectory after transfixion disappears. The trajectory immediately after transfixion was clearly visible as a white line in US images. However, 3 days after transfixion, the trajectory was nearly invisible, to the extent that it was difficult to imagine that the barely visible line was the trajectory of the previous transfixion.

The approximate costs of direct 3D printing of the vertebrae and trachea were $60 (US dollars) and $10, respectively. The initial total cost of 3D printing of the required molds was high—approximately $1650. The approximate costs per mold were as follows: blood vessels, $30; thyroid gland, $40; tumor, $10; and outer frame, $1500. The total cost of the chemicals used for fabrication of organs was negligible—approximately $4 (breakdown: blood vessels, $0.1; thyroid gland, $1; tumor, $0.1; and surrounding soft tissue, $1). A summary of the cost of materials and printing is presented in the Table. The cost of reproducing the same phantom is low—approximately $4. If the molds for the vertebrae and trachea can be printed once, and these components can be cast with a nonpermeable compound—such as a cement-based material—the approximate cost can be further reduced to $4 per model. Furthermore, the cost of fabricating a phantom from the CT data of another patient could be relatively low if the same outer frame is used for each phantom and only the patient-specific internal organs are custom fabricated.

In response to question 1 of the questionnaire survey administered to 10 medical specialists and 30 medical students who practiced thyroid gland transfixion with our model, all 45 participants replied that they found the phantom to be useful for clinical training. In response to question 2, 30 participants, excluding the specialists, professed increased interest in thyroid diseases after using the phantom (Fig. 3).

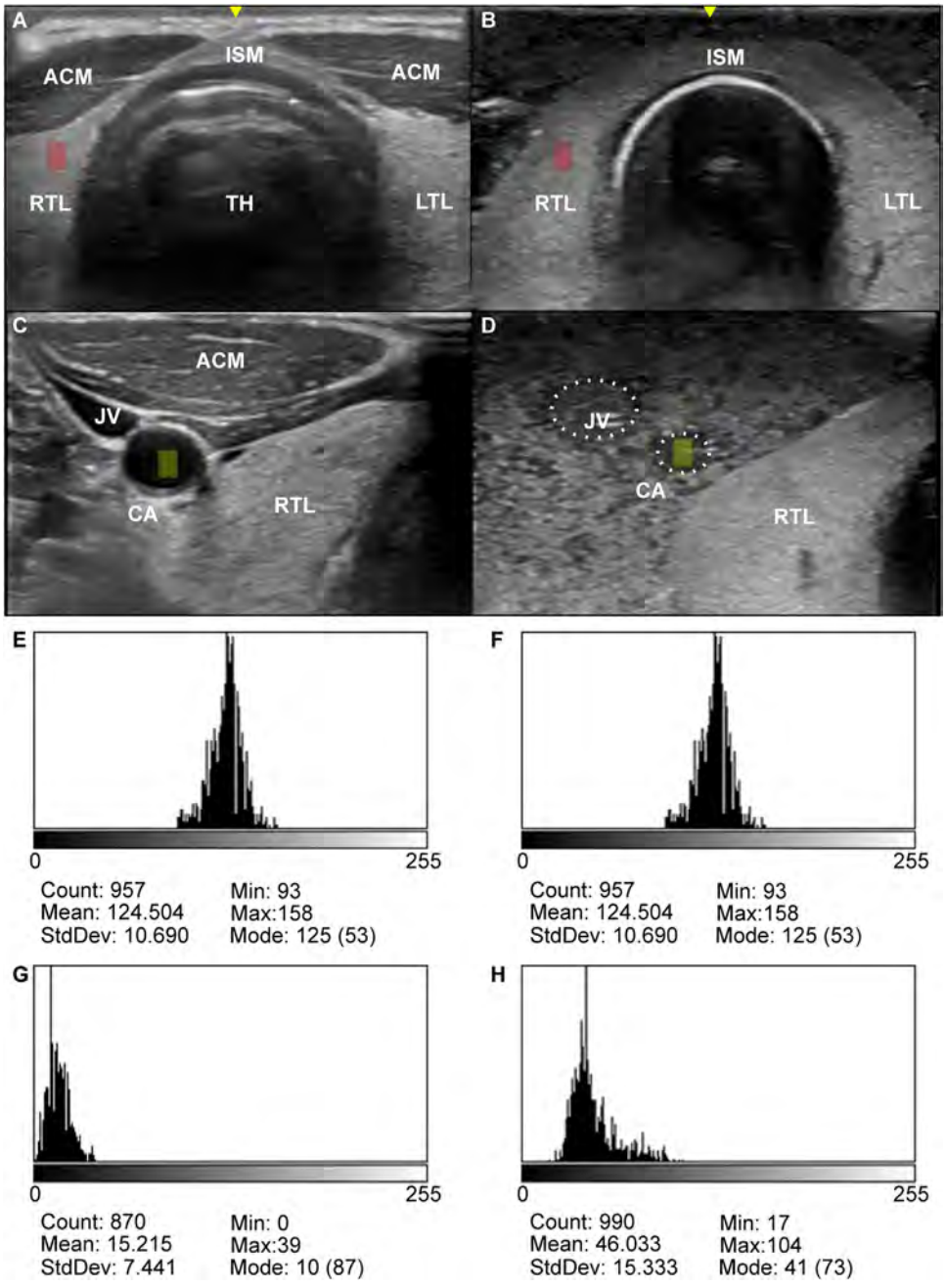

FIGURE 2. Ultrasonography images of the thyroid gland (A and B) and vascular structure of the carotid artery or jugular vein (C and D) of the neck of a human subject (A and C) and the phantom (B and D). Histogram of luminescence of the thyroid gland (E and F) and vascular structures (G and H) of the neck of the human subject (E and G) and the phantom (F and H). ACM, anterior cervical muscle; CA, carotid artery; ISM, isthmus; JV, jugular vein; LTH, left thyroid lobe; RTL, right thyroid lobe; TH, trachea.

DISCUSSION

The concept of textbooks and learning materials has changed in recent years. Until the previous decade, "learning" referred mainly to "studying through books". However, in recent times, the use of such mediums as virtual reality and lifelike models (realistic phantoms) provide learning and practice through a mechanism that is significantly closer to the actual experience.

Phantoms are used for medical training in various fields, including pediatrics and in the diagnosis of breast and thyroid gland diseases. However, there is a remarkable variation in the quality of materials used for fabricating phantoms—studies have reported tofu,[9] gelatin,[10] agar,[11] premisorb,[12] silicone,[13] and cadaver-based[14] phantoms. In the present study, the primary materials used for fabrication of the phantom were agar and sodium alginate.

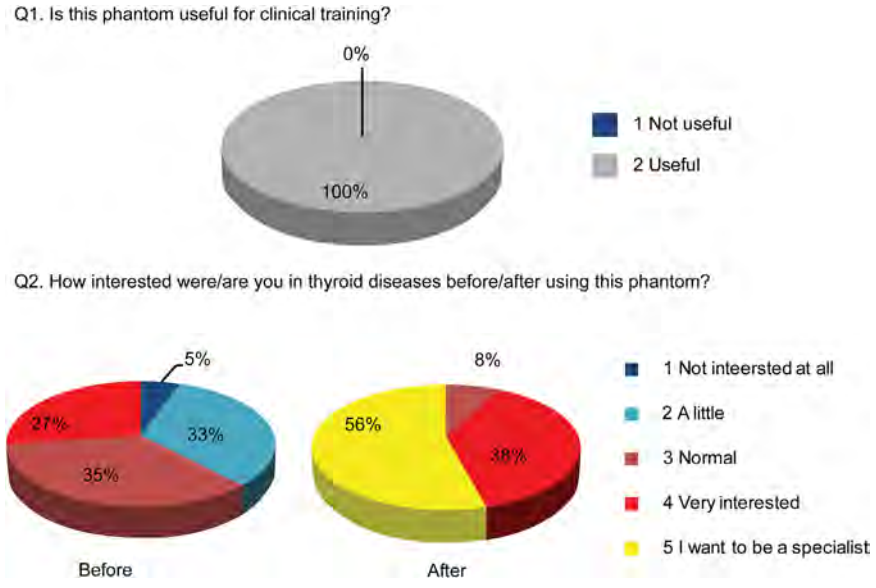

FIGURE 3. The results of the questionnaire survey. Question 1 was posed to all 45 participants, whereas question 2 was addressed to only 30 participants, excluding the specialists. All 45 participants replied that they found the phantom model useful. In response to question 2, all 30 medical students professed increased interest in thyroid diseases after using the phantom.

This study aimed ideally to fabricate a low-cost fully tailored phantom, to achieve which, we chose to use 2 different methods for fabricating the framework and organs to be punctured. Fabrication of a tailored phantom requires CT data of human neck. Therefore, 3D printing with data acquired from imaging the human neck is essential to fabricate a precise tailored phantom. However, 3D printing has a few limitations in terms of cost and currently available 3D-printable materials with ultrasound permeability. Currently available 3D-printable materials are highly ultrasound-reflective because of their nonpermeability, which inhibits US transparency. Although high reflectivity was acceptable for the trachea and bone structure, it was unacceptable for the remaining components required for the tailored thyroid gland phantom. To address this issue, we fabricated the framework and organs by different methods using a 3D printer and certain specific materials and successfully fabricated a cost-effective, ultrasonographically accurate phantom that can be used repeatedly.

Typically, 3D printers function by printing out successive layers of resin to convert digital data to a physical 3D representation of the digital model. They are widely used for academic and commercial applications. In the medical field, 3D printers are used to create organ models and bone structures.[15] These models are used to assist in the education and training of medical staff.[16] Tailored phantoms of individual patients can be created to confirm the feasibility and safety of proposed treatments as well as to facilitate practice of the procedure before actual treatment, which is of particular importance to inexperienced medical staff. Significant research is ongoing in this emerging field; for example, studies have reported the fabrication phantoms of the breast,[17] liver,[18] uterus, and vagina.[19] However, studies involving the use of 3D printers for fabrication of phantoms are limited,[20] which might be related to the current limitations in the availability of 3D-printable materials with ultrasound permeability. For this reason, we created most of the thyroid gland components from 3D-printed molds into which a compound that provided the required level of ultrasound permeability was injected or poured. We were thus able to fabricate an elaborate phantom with US authenticity and lifelike elasticity at a very reasonable cost.

In the present study, agar was one of the major components of the polymers poured into the mold. We chose agar because of its low cost and ability to be manipulated in terms of gelling speed and mechanical and US properties by the addition of various compounds. Although the initial cost of 3D printing of molds in the present study was high, the cost of reproducing the fabricated phantom using same mold was reasonable. A report summarizing the characteristics of several materials had noted that agar is not easily available.[21] However, in Japan, agar is readily available at a low cost. Furthermore, once the molds have been fabricated, no special equipment is required beyond the provision of a heat source and refrigeration, which allows fabrication of the phantom even in the absence of special instruments and conditions. Another advantage is the elasticity and strength of the phantom, which can be easily modified by adjusting the concentration of agar. In the present study, a 3% solution was chosen as the ideal concentration of agar after a few attempts. Our phantom was sufficiently robust to be

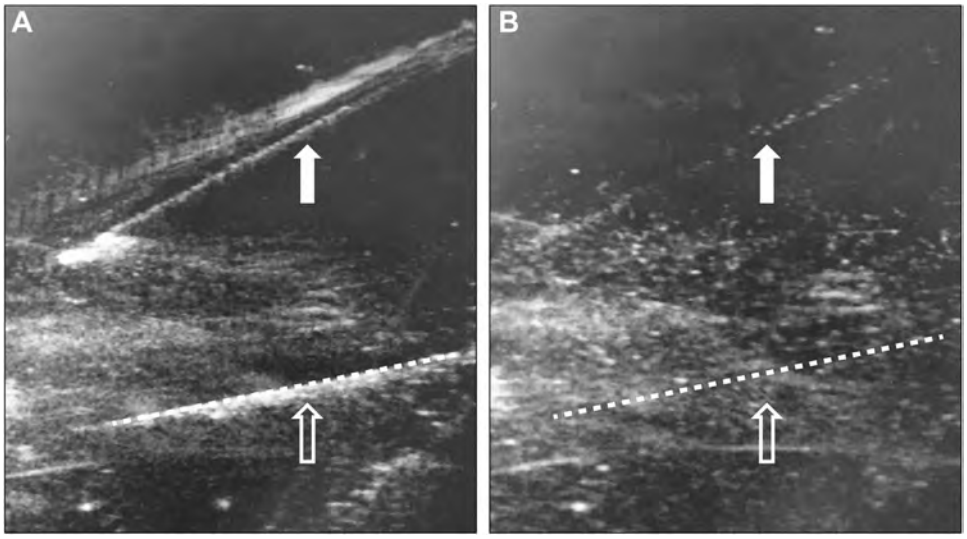

FIGURE 4. Trajectory of transfixion. Trajectory marks immediately after transfixion (A) and on day 3 after transfixion (B). The upper transfixion line (white arrow) was still slightly visible at day 3 after transfixion. In contrast, the lower transfixion line (open arrow and dotted line) had almost disappeared by the time of ultrasonography.

transfixed by 10 medical specialists without any damages other than needle tracks. With regard to elasticity, although agar gel is projected as being hard, addition of appropriate compounds can provide agar gel a skin-like haptic feel.

Another important material used for fabrication of the thyroid gland and surrounding soft tissue in the present study was sodium alginate, which has the same base material as agar. It is a convenient material for creating gelatinous compounds. Sodium alginate offers the advantage of manipulation of gelling speed by varying the concentration of the additive, dicalcium phosphate; sodium alginate gel solidifies upon the addition of dicalcium phosphate. Because of the low viscosity of agar solution, bubbles rise to the surface and dissipate. However, in case of a highly viscous solution like that of sodium alginate, gelling occurs almost instantaneously, causing bubbles to be trapped in the gel. The presence of air bubbles in the phantom has a negative effect on its US characteristics (data not shown). To avoid this issue, the process of gelling should be performed under pressure at a higher temperature, and an antifoaming agent should ideally be incorporated into the gel. However, it is easy to control the gelling speed with the procedure outlined in this article—sodium alginate is first added to alcohol, the alcoholic solution is then mixed with water, sodium pyrophosphate is added to this solution to form a gel, and finally, glucono-δ-lactone is added to adjust the gelling speed. This procedure requires minimal equipment and materials.

The most difficult aspect in the fabrication of this prototype phantom was the balance between mechanical strength for haptic authenticity and appropriate echo luminescence for US authenticity to ensure realistic transfixion training. Although increasing the concentration of solute increases the strength of the polymer, it results in excessive luminescence and increased the number and cost of ingredients required. In case of the thyroid gland, addition of agar to ethanol increased the viscosity of the solution, thus providing additional strength to the agar gel. In case of the surrounding soft tissue, the use of agar alone provided insufficient US luminescence, as mentioned previously; addition of sodium alginate to this solution increased its luminescence. The use of high-elasticity agar was partially prompted by the need to minimize the traces left by transfixion. In our tests, although transfixion marks persisted in the phantom, they become less prominent with time (Fig. 4).

Recent studies have correlated the increase in diagnostic rate of thyroid diseases with increase in training.[7] In addition to its possible clinical applications, our training model for ultrasound-guided thyroid nodule FNAC also increased the interest of medical students in thyroid diseases, which could lead to an increase in the number of thyroid specialists and contribute to improvement in quality of FNAC in a clinical setting. However, to address the need for clinical evaluation of this phantom, we plan on evaluating the improvement in FNAC skills brought about by our phantom among medical personnel in the future.

In conclusion, we have described an original, low-cost, elaborate thyroid gland phantom, which can be fabricated in approximately 15 minutes and is ready for use after approximately 2 hours of refrigeration. Once the molds are fabricated using a 3D printer, the phantom is easy to duplicate at a low cost, without the need for any special skills or equipment. The US characteristics of the phantom were remarkably similar in terms of structure and

luminescence to those of the actual subject that the phantom was modeled after. This phantom can be reused several times for training purposes. Although our findings require re-verification, we expect this phantom to serve as an effective and fully tailored training model for thyroid gland transfixion practice.

REFERENCES

1. Li JW, Karmakar MK, Xi L, Kwok WH, Ngan Kee WD. Gelatin-agar lumbosacral spine phantom: a simple model for learning the basic skills required to perform real-time sonographically guided central neuraxial blocks. *J Ultrasound Med*. 2011;30(2):263-272.
2. Lèguevaque P, Motton S, Courbon F, Ricard M, Berry I, Querleu D. Evaluation of a trainer phantom in the learning phase of sentinel lymph node identification in breast cancer. *World J Surg*. 2011;35(5):995-1001.
3. Richardson C, Bernard S, Dinh VA. A cost-effective, gelatin-based phantom model for learning ultrasound-guided fine-needle aspiration procedures of the head and neck. *J Ultrasound Med*. 2015;34(8):1479-1484.
4. Frates MC, Benson CB, Charboneau JW, et al. Management of thyroid nodules detected at US: society of radiologists in ultrasound consensus conference statement. *Radiology*. 2005;237(3):794-800.
5. Cibas ES, Alexander EK, Benson CB, et al. Indications for thyroid FNA and pre-FNA requirements: a synopsis of the national cancer institute thyroid fine-needle aspiration state of the science conference. *Diagn Cytopathol*. 2008;36(6):390-399.
6. American Thyroid Association (ATA) Guidelines Taskforce on Thyroid Nodules and Differentiated Thyroid Cancer, Cooper DS, Doherty GM, et al. Revised American Thyroid Association management guidelines for patients with thyroid nodules and differentiated thyroid cancer. *Thyroid*. 2009;19(11):1167-1214.
7. Beland MD, Anderson TJ, Atalay MK, Grand DJ, Cronan JJ. Resident experience increases diagnostic rate of thyroid fine-needle aspiration biopsies. *Acad Radiol*. 2014;21(11):1490-1494.
8. Schneider CA, Rasband WS, Eliceiri KW. NIH Image to ImageJ: 25 years of image analysis. *Nat Methods*. 2012;9(7):671-675.
9. Pollard BA. New model for learning ultrasound-guided needle to target localization. *Reg Anesth Pain Med*. 2008;33(4):360-362.
10. Nicholson RA, Crofton M. Training phantom for ultrasound guided biopsy. *Br J Radiol*. 1997;70(830):192-194.
11. Baranauskas MB, Margarido CB, Panossian C, Silva ED, Campanella MA, Kimachi PP. Simulation of ultrasound-guided peripheral nerve block: learning curve of CET- SMA/HSL Anaesthesiology residents. *Rev Bras Anestesiol*. 2008;58(2):106-111.
12. Liu Y, Glass NL, Power RW. Technical communication: new teaching model for practicing ultrasound-guided regional anesthesia techniques: no perishable food products! *Anesth Analg*. 2010;110(4):1233-1235.
13. Niazi AU, Ramlogan R, Prasad A, Chan VW. A new simulation model for ultrasound-aided regional anesthesia. *Reg Anesth Pain Med*. 2010;35(3):320-321.
14. Tsui BC, Dillane D, Walji AH. Cadaveric ultrasound imaging for training in ultrasound-guided peripheral nerveblocks: upper extremity. *Can J Anaesth*. 2007;54(5):392-396.
15. Sugimoto M. Bio-Texture Modeling of realistic tangible 3D organ modeling in navigation and simulation for organ transplantation biology. *Organ Biol*. 2014;21(2):141-144.
16. Takagi K, Nanashima A, Abo T, et al. Three-dimensional printing model of liver for operative simulation in perihilar cholangiocarcinoma. *Hepatogastroenterology*. 2014;61(136):2315-2316.
17. Gresens AA, Britt RC, Feliberti EC, Britt LD. Ultrasound-guided breast biopsy for surgical residents: evaluation of a phantom model. *J Surg Educ*. 2012;69(3):411-415.
18. Sugimoto K, Moriyasu M, Shiraishi J, Yamada M, Imai Y. A phantom study comparing ultrasound-guided liver tumor puncture using new real-time 3D ultrasound and conventional 2D ultrasound. *AJR Am J Roentgenol*. 2011;196(6):W753-W757.
19. Nattagh K, Siauw T, Pouliot J, Hsu IC, Cunha JA. A training phantom for ultrasound-guided needle insertion and suturing. *Brachytherapy*. 2014;13(4):413-419.
20. West SJ, Mari JM, Khan A, et al. Development of an ultrasound phantom for spinal injections with 3-dimensional printing. *Reg Anesth Pain Med*. 2014;39(5):429-433.
21. Farjad Sultan S, Shorten G, Iohom G. Simulators for training in ultrasound guided procedures. *Med Ultrason*. 2013;15(2):125-131.